Source size and temporal coherence requirements of coded aperture type x-ray phase contrast imaging systems.

Peter R.T. Munro, Konstantin Ignatyev, Robert D. Speller and Alessandro Olivo

Department of Medical Physics and Bioengineering, University College London, Malet Place, Gower Street, London WC1E 6BT

p.munro@ucl.ac.uk

Abstract: There is currently much interest in developing X-ray Phase Contrast Imaging (XPCI) systems which employ laboratory sources in order to deploy the technique in real world applications. The challenge faced by nearly all XPCI techniques is that of efficiently utilising the x-ray flux emitted by an x-ray tube which is polychromatic and possesses only partial spatial coherence. Techniques have, however, been developed which overcome these limitations. Such a technique, known as coded aperture XPCI, has been under development in our laboratories in recent years for application principally in medical imaging and security screening. In this paper we derive limitations imposed upon source polychromaticity and spatial extent by the coded aperture system. We also show that although other grating XPCI techniques employ a different physical principle, they satisfy design constraints similar to those of the coded aperture XPCI.

OCIS codes: (050.1960) Diffraction theory; (110.7440) X-ray imaging;(120.5050) Phase measurement;

References and links

1. E. Castelli, F. Arfelli, D. Dreossi, R. Longo, T. Rokvic, M. Cova, E. Quaia, M. Tonutti, F. Zanconati, A. Abrami, V. Chenda, R. Menk, E. Quai, G. Tromba, P. Bregant, and F. de Guarrini, "Clinical mammography at the SYRMEP beam line," Nucl. Instrum. Meth. A **572**(1), 237 – 240 (2007).
2. A. Momose, W. Yashiro, Y. Takeda, Y. Suzuki, and T. Hattori, "Phase Tomography by X-ray Talbot Interferometry for Biological Imaging," Jpn. J. Appl. Phys. **45**, 5254–5262 (2006).
3. F. Pfeiffer, T. Weitkamp, O. Bunk, and C. David, "Phase retrieval and differential phase-contrast imaging with low-brilliance X-ray sources," Nat. Phys. **2**(4), 258–261 (2006).
4. S. Wilkins, T. Gureyev, D. Gao, A. Pogany, and A. Stevenson, "Phase-contrast imaging using polychromatic hard X-rays," Nature **384**, 335–338 (1996).
5. D. Chapman, W. Thomlinson, R. Johnston, D. Washburn, E. Pisano, N. Gmür, Z. . Zhong, R. Menk, F. Arfelli, and D. Sayers, "Diffraction enhanced x-ray imaging," Phys. Med. Biol. **42**(11), 2015 (1997).
6. Y. Suzuki, N. Yagi, and K. Uesugi, "X-ray refraction-enhanced imaging and a method for phase retrieval for a simple object," J. Synchrotron Radiat. **9**(3), 160–165 (2002).
7. A. Olivo and R. Speller, "Modelling of a novel x-ray phase contrast imaging technique based on coded apertures," Phys. Med. Biol. **52**(22), 6555–6573 (2007).
8. A. Momose, S. Kawamoto, I. Koyama, Y. Hamaishi, K. Takai, and Y. Suzuki, "Demonstration of X-Ray Talbot Interferometry," Jpn. J. Appl. Phys. **42**(Part 2, No. 7B), L866–L868 (2003).
9. T. Weitkamp, A. Diaz, C. David, F. Pfeiffer, M. Stampanoni, P. Cloetens, and E. Ziegler, "X-ray phase imaging with a grating interferometer," Opt. Express **13**(16), 6296–6304 (2005).
10. F. Pfeiffer, M. Bech, O. Bunk, P. Kraft, E. F. Eikenberry, C. Bronnimann, C. Grunzweig, and C. David, "Hard-X-ray dark-field imaging using a grating interferometer," Nat. Mater. **7**(2), 134–137 (2008).

#127840 - $15.00 USD Received 30 Apr 2010; revised 27 Jul 2010; accepted 29 Jul 2010; published 1 Sep 2010

11. A. Olivo and R. Speller, "A coded-aperture technique allowing x-ray phase contrast imaging with conventional sources," Appl. Phys. Lett. **91**(7), 074,106 (2007).
12. Z.-F. Huang, K.-J. Kang, L. Zhang, Z.-Q. Chen, F. Ding, Z.-T. Wang, and Q.-G. Fang, "Alternative method for differential phase-contrast imaging with weakly coherent hard x rays," Phys. Rev. A **79**(1), 013,815 (2009).
13. A. Olivo and R. Speller, "Image formation principles in coded-aperture based x-ray phase contrast imaging," Phys. Med. Biol. **53**(22), 6461–6474 (2008).
14. X. Wu and H. Liu, "A new theory of phase-contrast x-ray imaging based on Wigner distributions," Med. Phys. **31**(9), 2378–2384 (2004).
15. L. Mandel and E. Wolf, *Optical Coherence and Quantum Optics* (Cambridge University Press, Cambridge, 1995).
16. M. Born and E. Wolf, *Principles of Optics*, seventh ed. (Cambridge University Press, Cambridge, 1999).
17. Y. I. Nesterets and S. W. Wilkins, "Phase-contrast imaging using a scanning-doublegrating configuration," Opt. Express **16**(8), 5849–5867 (2008).
18. P. Munro, R. Ignatyev, K. Speller, and A. Olivo, "The relationship between wave and geometrical optics models of coded aperture type x-ray phase contrast imaging systems," Opt. Express **18**(5), 4103–4117 (2010).
19. E. Chu, *Discrete and Continuous Fourier Transforms: Analysis, Applications and Fast Algorithms* (Chapman and Hall/CR, 2008).
20. R. Nowotny and A. Höfer, "A computer code for the calculation of diagnostic x-ray spectra," Fortschr Röntgenstr **142**, 685–689 (1985).
21. M. Engelhardt, C. Kottler, o. Bunk, C. David, C. Schroer, J. Baumann, m. Schuster, and F. Pfeiffer, "The fractional Talbot effect in differential x-ray phase-contrast imaging for extended and polychromatic x-ray sources," J. Microsc. **232**, 145–157 (2008).

1. Introduction

Phase sensitive x-ray images have a significantly higher quality than conventional absorption based x-ray images. For just a few examples of such images, see Refs [1–7]. X-ray phase contrast imaging (XPCI) techniques traditionally fall into three broad categories. One category is characterised by the use of an analyzer crystal whose rocking curve is used to generate intensity modulation from small angular deviations of photons [5]. This technique requires a highly collimated, monochromatic beam and so is most practically performed using synchrotron radiation. Another category generates intensity modulation by interference between waves reaching the detector without being perturbed by a sample with those which have been perturbed [4, 6]. The technique requires that a gap be introduced between the sample and the detector and also that a source of high spatial coherence is employed. For this reason, the technique is generally used with synchrotron radiation or microfocal sources. The third category may be broadly described as grating interferometry which employs a combination of phase and transmission gratings to perform wavefront sensing. All manifestations of this technique make use of Talbot's self imaging phenomenon and thus impose restrictions on source coherence in order that the diffracted orders of the grating interfere. This technique has been employed using synchrotron sources [8, 9] and laboratory sources [3, 10].

Our group has developed an XPCI technique which employs gratings but is, however, non-interferometric [11]. We believe that this technique, known as Coded Aperture XPCI (CAXPCI), thus forms part of a different category of XPCI systems. It would appear that the technique recently developed by Huang *et al.* [12] also fits within this category. The image formation principles of CAXPCI are explained by Olivo and Speller [13] however we present a summary here to establish the basis of this paper. Schematic diagrams of a CAXPCI system sensitive to phase gradients in one dimension are shown in Fig. 1. The diagram demonstrates how G_1 generates discrete x-ray beams which are incident upon G_2. G_2 has a pitch P and G_1 has a pitch P/M where M is the magnification defined as $M = (z_{so} + z_{od})/z_{so}$ where z_{so} and z_{od} are the distance from the source to G_1 and from G_1 to the detector respectively. Both gratings have the same fill factor. Thus, if a point source were employed and diffraction neglected, the gratings could be offset by adjusting ΔP in such a way that none, all or some fraction of photons admitted by G_1 reach the detector. The case where a fraction of the photons reach the detector is of most

#127840 - $15.00 USD Received 30 Apr 2010; revised 27 Jul 2010; accepted 29 Jul 2010; published 1 Sep 2010

importance as this constitutes the phenomenon of pixel edge illumination [13]. Note that we assume that the detector is aligned such that the centre of each pixel coincides with the centre of a transmitting region of G_2. Furthermore, it is assumed that when G_2 is translated with respect to G_1, the detector is translated in accordance with G_2. The principle of pixel edge illumination

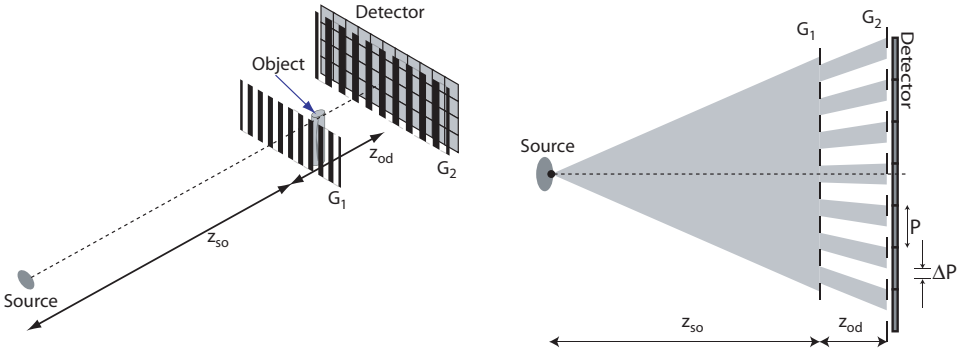

Fig. 1. Schematic diagrams of a CAXPCI system. The diagram on the right is a top-down version of the left. G_1 and G_2 are both transmission gratings. G_1 creates x-ray beams which are incident upon G_2 which is used to achieve partial pixel illumination.

is depicted in Fig. 2. The left diagram of Fig. 2 shows how x-ray photons may be refracted into the sensitive region of the pixel thus increasing the detected signal. The right diagram of Fig. 2 shows how x-ray photons can be refracted away from the sensitive region of the detector thus reducing the detected signal. A profile of the sample may be obtained using a single detector pixel by recording the signal for a range of sample scan positions. In order to reduce the need for scanning the object, a number of aperture pairs may be employed in parallel as shown in Fig. 1.

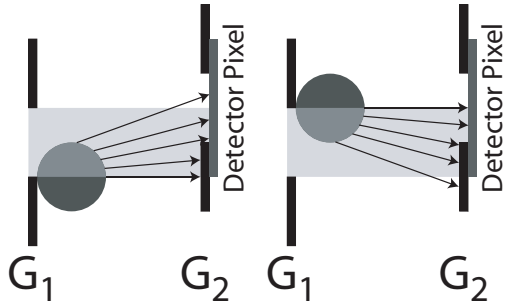

Fig. 2. Diagrams showing the principle of pixel edge illumination with a cylindrical sample. The pixel edge refers to the edge of the region of the pixel not covered by G_2. The left diagram would result in an increased detector signal whilst the right would result in a reduced signal. It is assumed that the real part of the refractive index of the cylinder is less than unity as is typical for materials of interest at x-ray photon energies. The arrows are intended to indicate the fraction of photons and note that the divergence of the x-ray beam has been neglected for simplicity.

CAXPCI can be performed according to a number of modalities. In particular, principally absorption images can be obtained by setting ΔP to 0 and dark field images may be acquired

#127840 - $15.00 USD Received 30 Apr 2010; revised 27 Jul 2010; accepted 29 Jul 2010; published 1 Sep 2010

by adjusting ΔP such that x-rays are not directly incident upon the detector. CAXPCI is, however, being developed for real world applications such as mammography where both phase and absorption information must be obtained. Phase stepping, as employed in Talbot interferometry [2, 3], is sometimes impractical in such applications so we opt to take a single acquisition for a value of ΔP which results in an image possessing both absorption and phase contrast. Furthermore, it is possible to extract sample phase and absorption information from two different CAXPCI images which is the subject of forthcoming publications.

This description of the technique makes a number of assumptions which need to be upheld for the technique to work in practice. For example, a conventional x-ray tube is employed in practice to enable the method to be applied to real world applications. Sources, as used in mammography for example, have a finite source spatial Full Width at Half Maximum (FWHM) which causes the intensity of the field incident upon G_2 to become less sharp with reduced intensity modulation. This loss of sharpness and modulation makes it more difficult to achieve pixel edge illumination and thus compromises the performance of the method. The objective of this paper is to analyse the requirements placed upon the source temporal coherence and size such that satisfactory pixel edge illumination may be achieved. This is done by deriving general equations for the field which results from diffraction by G_1 for a realistic x-ray source. These equations are then used to predict the performance of the CAXPCI system as the source temporal coherence and size varies. Finally, we demonstrate the salient differences between the CAXPCI method and interferometric grating based techniques.

2. Calculation of the field intensity incident upon the detector

In this section we derive an expression for the intensity of x-rays incident upon grating G_2 for the system depicted in Fig. 1. The anode of an x-ray tube may be considered the source of a partially coherent field [14]. What follows is rigorously explained elsewhere [15, 16] however we provide a brief account as introductory material. Note also that a general account of this theory for XPCI systems is given by Nesterets and Wilkins [17]. Assuming that the fluctuating field of the source is statistically stationary, the cross-spectral density of the field, $W(\mathbf{r}_1, \mathbf{r}_2, \omega)$, may be rigorously expressed as the cross correlation of an ensemble of monochromatic realizations $U(\mathbf{r}, \omega)\exp(-i\omega t)$ [15]. This is expressed mathematically as:

$$W(\mathbf{r}_1, \mathbf{r}_2, \omega) = \langle U^*(\mathbf{r}_1, \omega) U(\mathbf{r}_2, \omega) \rangle_\omega$$

where * represents complex conjugation, $\mathbf{r}_1$ and $\mathbf{r}_2$ are position vectors, ω is the angular frequency of oscillation and, as in Mandel and Wolf [15], the subscript ω is attached to stress that the average is taken over an ensemble of space-frequency realizations. We will not attempt to determine the ensemble, we note only that it exists. This theory may be employed to calculate the spectral density which results when a x-ray tube source illuminates a thin grating, either phase or transmission. A monochromatic realization at the source, $U(x_s, \omega; -z_{so})$, will result in a transmitted field:

$$U(x_d, \omega; z_{od}) = \int_\sigma K(x_d, x_s, \omega; z_{os}, z_{od}) U(x_s, \omega; -z_{so}) \mathrm{d}x_s$$

where $K(x_d, x_s, \omega; z_{os}, z_{od})$ describes the transmitted field for a monochromatic point source of angular frequency ω, with unit amplitude located at position x_s on the source and σ is the surface defined by the source. The cross-spectral density of the transmitted field may then be found according to [15]:

$$\begin{aligned} W(x_{d1}, x_{d2}, \omega) &= \langle U^*(x_{d1}, \omega; z_{od}) U(x_{d2}, \omega; z_{od}) \rangle_\omega \\ &= \int_\sigma \int_\sigma K^*(x_{d1}, x_{s1}, \omega; z_{os}, z_{od}) K(x_{d2}, x_{s2}, \omega; z_{os}, z_{od}) \langle U^*(x_{s1}, \omega; -z_{so}) U(x_{s2}, \omega; -z_{so}) \rangle_\omega \mathrm{d}x_{s1} \mathrm{d}x_{s2} \end{aligned} \quad (1)$$

#127840 - $15.00 USD Received 30 Apr 2010; revised 27 Jul 2010; accepted 29 Jul 2010; published 1 Sep 2010

This expression may be simplified by noting that it may be reasonably approximated that two distinct elements of the source should be uncorrelated [15], allowing us to write:

$$\begin{aligned} W(x_{s1},x_{s2},\omega) &= \langle |U(x_{s1},\omega)|^2 \rangle_\omega \delta(x_{s1}-x_{s2}) \\ &= I(x_{s1},\omega)\delta(x_{s1}-x_{s2}) \end{aligned} \quad (2)$$

where δ is Dirac's delta function and $I(x_{s1},\omega)$ is the intensity of the field at angular frequency ω. Substituting Eq. (2) into Eq. (1) then yields:

$$W(x_{d1},x_{d2},\omega) = \int_\sigma K^*(x_{d1},x_{s1},\omega;z_{os},z_{od})K(x_{d2},x_{s1},\omega;z_{os},z_{od})I(x_{s1},\omega)\mathrm{d}x_{s1}$$

and if we seek only the intensity of the transmitted field this further simplifies to

$$I(x_{d1},\omega) = \int_\sigma |K(x_{d1},x_{s1},\omega;z_{os},z_{od})|^2 I(x_{s1},\omega)\mathrm{d}x_{s1}$$

which may be integrated over ω to obtain the total intensity as:

$$I(x_{d1}) = \frac{1}{2\pi}\int_0^\infty \int_\sigma |K(x_{d1},x_{s1},\omega;z_{os},z_{od})|^2 I(x_{s1},\omega)\mathrm{d}x_{s1}\mathrm{d}\omega \quad (3)$$

We showed in a recent publication [18] that, for a grating with transmission function described as $T(\xi)=\sum_{n=-\infty}^{\infty} C_n \exp(in\xi/L)$, $K(x_{d1},x_{s1},\omega;z_{os},z_{od})$ may be defined as:

$$\begin{aligned} K(x_{d1},x_{s1},\omega;z_{os},z_{od}) &= \frac{\exp\left(ik(z_{so}+z_{od})\right)}{z_{so}+z_{od}} \exp\left(ik\frac{(x_{d1}-x_{s1})^2}{2(z_{so}+z_{od})}\right)\cdot \\ &\sum_{n=-\infty}^{\infty} \exp\left(-i\pi\lambda\left(\frac{n}{L}\right)^2\frac{z_{so}z_{od}}{z_{so}+z_{od}}\right) C_n \exp\left(i2\pi\frac{n}{L}x'\frac{z_{so}}{z_{so}+z_{od}}\right) \end{aligned} \quad (4)$$

where $x' = x_{d1}+x_{s1}z_{od}/z_{so}$, $k=2\pi/\lambda$ and $\omega = kc$. This expression is obtained by applying the paraxial (ie, small angle) approximation to the Fresnel-Kirchhoff diffraction integral [16]. In order to employ this result in Eq. (3) we make some further assumptions regarding the x-ray tube source. In particular, we assume that the source intensity may be described by

$$I(x_s,\omega) = \frac{1}{\sigma_x\pi}\exp\left[-\left(\frac{x_s}{\sigma_x}\right)^2\right] I(\omega) \quad (5)$$

where, in general, $I(\omega)$ can be calculated approximately depending upon factors such as the anode type, anode angle, filtration and tube voltage and σ_x is related to the source spatial FWHM by $\sigma_x = \mathrm{FWHM}/(2\sqrt{\log 2})$. Introducing Eqs. (5) and (4) into Eq. (3) yields

$$\begin{aligned} I(x_d) &= \frac{1}{(z_{so}+z_{od})^2}\sum_{n_1=-\infty}^{\infty}\sum_{n_2=-\infty}^{\infty}\left[\exp\left(-\pi^2\sigma_x^2\left(\frac{n_1-n_2}{L}\right)^2\left(\frac{z_{od}}{z_{so}+z_{od}}\right)^2\right)\right. \\ &\cdot\exp\left(i2\pi\left(\frac{n_1}{L}-\frac{n_2}{L}\right)\left(x_d\frac{z_{so}}{z_{so}+z_{od}}\right)\right) \\ &\left.\cdot C_{n_1}C_{n_2}^* c\int_{\lambda_s}^{\lambda_l}\exp\left(-i\pi\lambda\left(\left(\frac{n_1}{L}\right)^2-\left(\frac{n_2}{L}\right)^2\right)\frac{z_{so}z_{od}}{z_{so}+z_{od}}\right)\frac{I(\lambda)}{\lambda^2}\mathrm{d}\lambda\right] \end{aligned} \quad (6)$$

where c is the speed of light in air and λ_s and λ_l are the shortest and longest wavelengths emitted by the source. Note that the grating is assumed to be non-dispersive. For convenience we make

#127840 - $15.00 USD Received 30 Apr 2010; revised 27 Jul 2010; accepted 29 Jul 2010; published 1 Sep 2010

the following definitions:

$$\begin{aligned} K_1(\sigma_x, n_1, n_2) &= \exp\left(-\pi^2\sigma_x^2\left(\frac{n_1-n_2}{L}\right)^2\left(\frac{z_{od}}{z_{so}+z_{od}}\right)^2\right) \\ K_2(x_d, n_1, n_2) &= \exp\left(i2\pi\left(\frac{n_1}{L}-\frac{n_2}{L}\right)\left(x_d\frac{z_{so}}{z_{so}+z_{od}}\right)\right) \\ K_3(n_1, n_2) &= c\int_{\lambda_s}^{\lambda_l}\exp\left(-i\pi\lambda\left(\left(\frac{n_1}{L}\right)^2-\left(\frac{n_2}{L}\right)^2\right)\frac{z_{so}z_{od}}{z_{so}+z_{od}}\right)\frac{I(\lambda)}{\lambda^2}\mathrm{d}\lambda \end{aligned}$$

The CAXPCI system [11] employs a transmission grating which has a transmission function which may be described by:

$$T(\xi+nL) = \begin{cases} 1 & L/2(1-\eta) < \xi \leq L/2(1+\eta) \\ 0 & \text{otherwise} \end{cases}$$

where η is the fill factor, L is the pitch and $0 \leq \xi < L$. $T(\xi)$ has complex Fourier series coefficients:

$$C_n = \begin{cases} \frac{(-1)^n}{\pi n}\sin(\pi n\eta) & n \neq 0 \\ \eta & n = 0 \end{cases}$$

As only a finite number of terms can be used when calculating Eq. (6), the Gibbs phenomenon leads to non physical features in the calculated intensity. This is particularly significant due to the $1/n$ dependence of the Fourier coefficients of the transmission grating. To overcome this we have written the grating transmission function as a Cesaro sum [19] resulting in the transmission function being written as $T(\xi) = \sum_{n=-N}^{N}\beta_n C_n \exp(in\xi/L)$ where $\beta_n = (N+1-|n|)/(N+1)$.

The degree of pixel edge illumination, described conceptually in Sec. (1), is expressed quantitatively by the Illuminated Pixel Fraction (IPF). For a particular displacement of G_2, the IPF is defined as the ratio of the number photons which reach the detector to the number of photons which reach the detector when G_2 and G_1 are aligned ($\Delta P = 0$ in Fig. 1). The signal detected by each detector pixel is calculated by integrating the intensity of x-rays transmitted by G_2 onto the pixel. This may be expressed mathematically for each pixel as:

$$I_{pix} = \int_0^P I(x_d)T\left(\frac{x_d-\Delta P}{M}\right)\mathrm{d}x_d$$

The IPF may then be calculated as:

$$\mathrm{IPF} = I_{pix}\Big/\int_0^P I(x_d)T\left(x_d/M\right)\mathrm{d}x_d$$

It has been shown previously [11] that the contrast of a CAXPCI system increases as the IPF decreases and so it is an important metric for such systems.

3. Analysis

The spectrum of an x-ray source is generally not known analytically. We have thus used a spectrum obtained using numerical calculation [20]. A sample spectrum is shown in Fig. 3 which corresponds to an x-ray tube with a tungsten anode, a tube voltage of 40 kV, 2mm of aluminium filtering, an anode angle of 17° calculated 10cm from the source. These parameters were chosen as an example of a spectrum which may be used in medical applications. We note also that we assume that the change in the spectrum due to propagation in air is assumed to

#127840 - $15.00 USD Received 30 Apr 2010; revised 27 Jul 2010; accepted 29 Jul 2010; published 1 Sep 2010

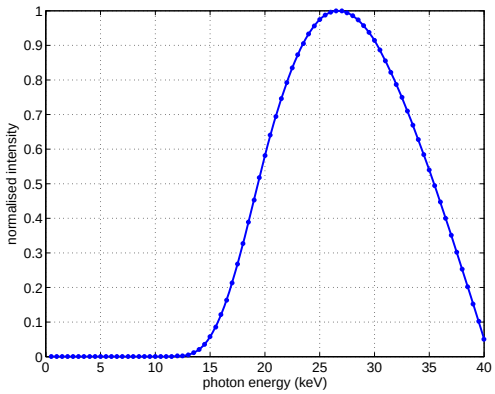

Fig. 3. Spectrum of x-rays emitted by an x-ray source with tube voltage of 40 kV for a tungsten anode, 2mm of aluminium filtration, an anode angle of 17° at a distance of 10cm from the source. Data was calculated by code developed by Nowotny and Höfer [20]. The mean photon energy is 27.4keV corresponding to wavelength 45pm.

have a negligible effect on the field at G_2. The results presented in this section are however not limited to this particular spectrum.

We first consider the intensity of x-rays incident upon G_2 in the case where an x-ray source emits photons with a spectrum as shown in Fig. 3 from a vanishingly small area on the anode. This scenario will not be encountered in practice, we consider it to highlight the impact of the temporal coherence of the source. When a point source is employed, K_1 in Eq. (6) becomes equal to unity. Fig. 4 shows the intensity of x-rays incident upon G_2 for three values of L, chosen to illustrate the three regimes under which contrast is created at G_2. Plots of the real and imaginary parts of K_3 are shown in Fig. 5. A typical CAXPCI system geometry of $z_{so} = 1.6$m and $z_{od} = 0.4$m and a grating fill factor of 0.5 was employed for these calculations. Before analysing Figs. (4) and (5) we compare the source coherence length to the propagation distance of each plane wave component inside the summation of Eq. (4). The nth component travels a distance of approximately $z_{od}(1+(\lambda^2/2)(n/L)^2 z_{so}/(z_{so}+z_{od}))$ in propagating from G_1 to G_2. The nth component will interfere with the 0th component if the difference in propagation distance does not exceed the coherence length of the source, defined as $\lambda_0^2/\Delta\lambda$ [15] where λ_0 is the mean wavelength of the source and $\Delta\lambda$ the width of the spectrum. Thus, for interference to occur the following condition must be satisfied:

$$\frac{\Delta\lambda}{2}\left(\frac{n}{L}\right)^2 \frac{z_{so}z_{od}}{z_{so}+z_{od}} < 1 \tag{7}$$

from which we define the parameter

$$\gamma_t = \frac{\Delta\lambda}{2L^2}\frac{z_{so}z_{od}}{z_{so}+z_{od}}$$

which we will show later plays an important role in determining the effect that source temporal coherence has on the ability to achieve satisfactory pixel edge illumination.

For L=800λ_0 in Figs. (4) and (5), $\gamma_t = 3.5\times10^3$ and Eq. (7) is not satisfied for any values of n. K_3 is thus very close to $\delta_{|n_1|,|n_2|}$, where δ is Kronecker's delta, meaning that interference only occurs between equal and opposite diffracted orders ($n_1 = -n_2$). Under these circumstances it can be shown that the spatially varying part of the x-ray intensity in Eq. (6) becomes

#127840 - $15.00 USD Received 30 Apr 2010; revised 27 Jul 2010; accepted 29 Jul 2010; published 1 Sep 2010

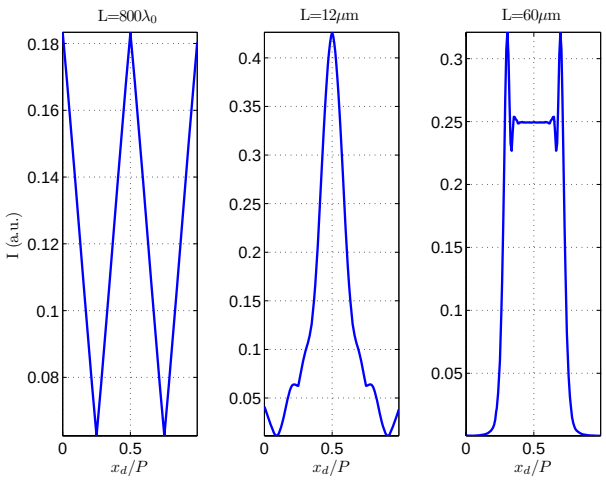

Fig. 4. Plots of x-ray intensity at the detector grating when a point source with the spectrum of Fig. 3 is employed for three values of L, $z_{so} = 1.6$m and $z_{od} = 0.4$m. λ_0 is 45pm, the wavelength of the mean photon energy.

a triangular pattern of peak to peak amplitude 1/8 as is closely resembled by the plot in Fig. 4. For L=12μm, $\gamma_t = 3.2 \times 10^{-2}$ and Eq. (7) is satisfied for small values of n. K_3 thus enables interference between diffracted orders n_1 and n_2 where $n_1^2 - n_2^2$ is small. Importantly, the diffracted orders acquire a phase term due to the differing propagation distances which results in a strongly perturbed intensity pattern as shown in Fig. 4. When L=60μm, $\gamma_t = 1.3 \times 10^{-3}$ and interference occurs between a large number of diffracted orders when compared with the other two examples. Furthermore, as shown in Fig. 5, K_3 approximates unity within a region described roughly by $\{(n_1,n_2)\big||n_1| \leq 5, |n_2| \leq 5\}$ meaning that a good replica of the aperture transmission function is produced at G_2 as shown in Fig. 4. Eq. (7) shows that increasing the the pitch (L) of G_1 mitigates the effect of a broad spectrum source. Further increasing L also improves the likeness between the intensity of x-rays at G_2 and the transmission profile of G_1 as the phase difference, due to propagation, between diffracted orders becomes negligible.

In order to further study the effect of source temporal coherence we consider the minimum achievable IPF (see Sec. (2)) assuming a pixel dimension (P) of 75μm, a total system length ($z_{so} + z_{od}$) of 2m and the spectrum shown in Fig. 3. These are typical system parameters as may be encountered in practice. The plot in Fig. 6 was calculated by varying z_{so} and z_{od}, subsequently varying the propagation distances of the diffracted orders. The plot shows that γ_t should be less than approximately 0.04 ($z_{so} = 0.229$m) in order to obtain a minimum achievable IPF of under 0.2, a threshold chosen on the basis of previous experimental results [11]. Practically speaking a value lower than this should be chosen as the minimum achievable IPF increases when a source of finite size is used.

We consider now the effect of the source size. If a point source is employed, K_1 becomes equal to unity for all values of n_1 and n_2 whilst if the source becomes large, K_1 tends to δ_{n_1,n_2}. For intermediate source sizes K_1 acts to dampen the effect of higher diffracted orders. It can be shown that, under general circumstances, the source size is more limiting than source bandwidth in producing a well modulated x-ray intensity pattern at G_2. We have previously built systems in our laboratory with pixel dimensions of 50μm, 85μm and 100μm with $z_{so} = 1.6$m, $z_{od} = 0.4$m with a source of FWHM measured to be 75μm. We have plotted K_1 against $|n_1 - n_2|$ for these

#127840 - $15.00 USD Received 30 Apr 2010; revised 27 Jul 2010; accepted 29 Jul 2010; published 1 Sep 2010

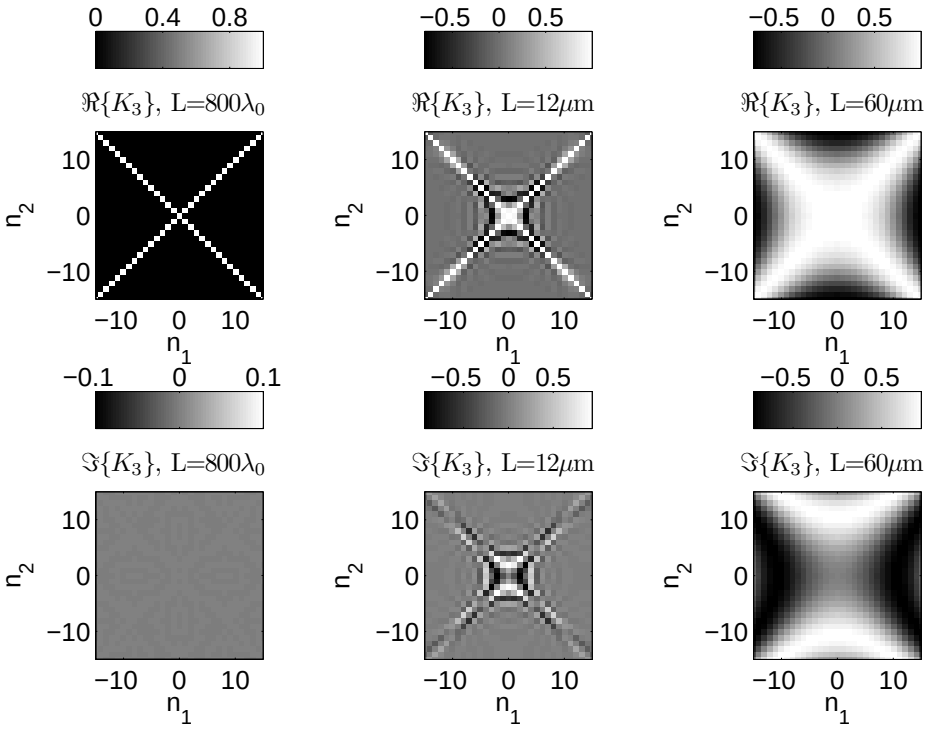

Fig. 5. Plots of the real ($\Re$) and imaginary ($\Im$) parts of K_3 calculated for three values of L, $z_{so} = 1.6$m and $z_{od} = 0.4$m for the spectrum shown in Fig. 3. λ_0 is 45pm, the wavelength of the mean photon energy. The chosen values of L result in values for γ_t of 3.5×10^{3}, 3.2×10^{-2} and 1.3×10^{-3} respectively.

parameters in Fig. 7. The plot shows that for these system parameters, K_1 is more restrictive than K_3, assuming the spectrum in Fig. 3, in terms of allowing interference between diffracted orders. Also, as expected, fewer diffracted orders are able to interfere for the smaller pitch gratings.

The definition of K_1 suggests the effect of the source size upon the intensity of x-rays at G_2 is described by the parameter:

$$\gamma_s = \frac{\sigma_x}{P}\frac{z_{od}}{z_{so}+z_{od}} = \frac{\sigma_x}{P}\frac{z_{od}}{z_{so}} \tag{8}$$

We calculated the minimum achievable IPF for varying σ_x, P, z_{so} and z_{od} for the spectrum shown in Fig. 3 whilst keeping the system length fixed at 2m. The range of parameters is explained in the caption of Fig. 8. As expected, a scatter plot of minimum IPF versus the parameter in Eq. (8) results in a plot where all points lie on a line as plotted in Fig. 8. This demonstrates the importance of the parameter defined in Eq. (8). The results show that γ_s should not exceed approximately 0.15 if the minimum achievable IPF is to remain below 0.2. It is also notable that the minimum achievable IPF reaches approximately 0.5 when the source size parameter reaches 0.3 and saturates at 1 when the size parameter reaches 1.

#127840 - $15.00 USD Received 30 Apr 2010; revised 27 Jul 2010; accepted 29 Jul 2010; published 1 Sep 2010

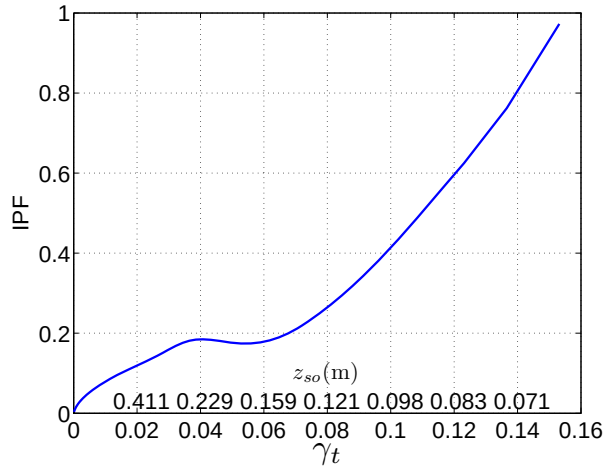

Fig. 6. Plot of minimum achievable IPF versus γ_t for a point source with spectrum as shown in Fig. 3. z_{so} and z_{od} were varied whilst maintaining $z_{so} + z_{od} = 2$m.

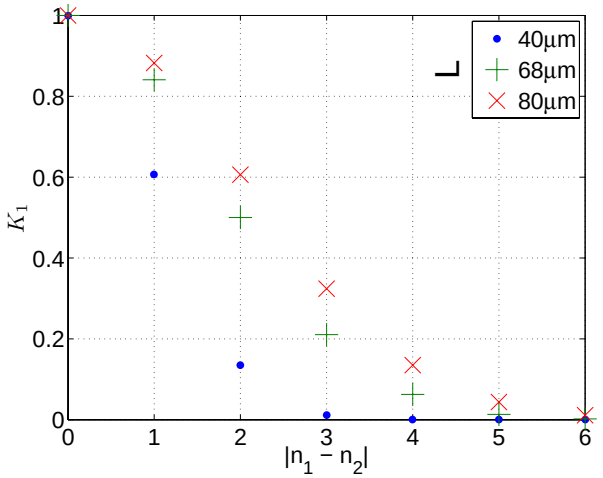

Fig. 7. Plot of K_1 for three typical values of L: $40\mu m$, $68\mu m$ and $80\mu m$ with $z_{so} = 1.6$m, $z_{od} = 0.4$m and a source FWHM of 75μm.

4. Discussion and conclusions

We have derived two metrics, γ_t and γ_s, which can be used to characterise the effect of source temporal coherence and size, respectively, upon the performance of a CAXPCI system. Relationships between these two metrics and minimum achievable IPF were derived. One of the main outcomes of this work is the demonstration of important differences between CAXPCI and other XPCI systems which employ gratings. It has already been explained in this paper and in previous publications [11, 13] that the novelty of CAXPCI is use of the pixel edge illumination phenomenon. Pixel edge illumination permits sensitivity to fine angular deviations of photons irrespective grating pitch. Thus employing a grating G_1 with pitch of between 60 and

#127840 - $15.00 USD Received 30 Apr 2010; revised 27 Jul 2010; accepted 29 Jul 2010; published 1 Sep 2010

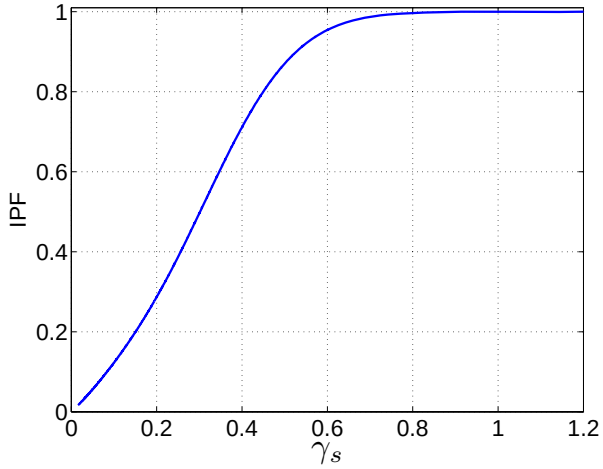

Fig. 8. Plot of minimum achievable IPF against γ_s. The IPF was calculated for combinations of P=50, 85 and 100μm, z_{so} varying between 1 and 1.9m, total system length equal to 2m, source FWHM varying between 50 and 100μm and the spectrum shown in Fig. 3. All resultant data points were found to lie on the line plotted in the figure.

80μm has some important implications. Firstly, it results in a value of $\gamma_s \approx 1.3 \times 10^{-3}$ which means that the effects of diffraction and source temporal coherence are largely mitigated due to the small angular deviation of diffracted orders. This is discussed in Sec. (3) and illustrated in Figs. (4) and (5). It is for this reason that we describe CAXPCI as non-interferometric. The polychromaticity of the source may in fact be regarded as beneficial as it smooths out the ripples in the field incident upon G_2 which would be present if a monochromatic source were employed. Alternative grating techniques characterised by the use of Talbot's self imaging phenomenon have been demonstrated and used to produce high quality phase contrast images [2,3]. These techniques are however interferometric as they require the system geometry and grating pitch to satisfy Talbot's condition for self imaging which is based upon developing a precise, non-negligible, phase difference between diffracted orders of G_1. This is demonstrated by considering the system reported by Pfeiffer *et. al* [3] which employs a phase grating for G_1 with $z_{so} = 1.765$m, $z_{od} = 27.8$mm and $L = 3.938\mu$m. For the same source spectrum considered in this paper, this results in $\gamma_t \approx 0.026$, an order of magnitude greater than that of the CAXPCI system resulting in a K_3 in the regime of the middle plots of Fig. 5. One could thus differentiate CAXPCI from Talbot based techniques by the result that CAXPCI is designed to make diffraction effects negligible and Talbot based techniques strictly control the effects of diffraction.

We also showed that to achieve an IPF of 0.2 the source size is limited by the relationship $\gamma_s < 0.15$ which according to the definition of γ_s, requires the source spatial FWHM to satisfy FWHM $< 0.25 z_{so}/z_{od} P$. This is an important relationship as one of the strengths of CAXPCI is that a phase contrast image may be obtained with a single exposure. In the case of CAXPCI, P is the detector pixel dimension as well as the pitch of G_2 as phase stepping is not employed. Thus, for a typical CAXPCI system geometry of $z_{so} = 1.6$m and $z_{od} = 0.4$m, the source FWHM is restricted to FWHM $< P$ which is achievable for the pixel dimensions of detectors employed in our laboratory. The same relationship must be observed by Talbot techniques using somewhat different system parameters. For the previously considered system by Pfeiffer *et. al* [3] employs a source grating to aperture the source, resulting in mutually incoherent line sources of width of between 25μm and 50μm [3]. Approximating a line source by a Gaussian profile with FWHM

#127840 - $15.00 USD Received 30 Apr 2010; revised 27 Jul 2010; accepted 29 Jul 2010; published 1 Sep 2010

equal to the width of the line source reveals that the particular Talbot XPCI system results in $5.9 \times 10^{-2} < \gamma_s < 1.2 \times 10^{-1}$.

Another result from this work is the demonstration that the CAXPCI system is more sensitive to the deleterious effects of a large source FWHM than a broad spectrum source. This is illustrated by comparing the plot of K_3 in the right hand axes of Fig. 5 with the plot of K_1 in Fig. 7. In particular, for the representative system parameters which were chosen, K_1 restricts the interference of diffracted orders more substantially than K_3. For example, the right hand axes of Fig. 5 show that strong interference with only small phase perturbations is possible for diffracted orders n_1 and n_2 approximately satisfying $|n_1| \leq 5$ and $|n_2| \leq 5$ when $L = 60\mu$m and the spectrum of Fig. 3 is employed. Fig. 7 however shows that a source with FWHM of just 75μm would allow strong interference between diffracted orders n_1 and n_2 approximately satisfying $|n_1 - n_2| \leq 1$, which is far more restrictive than the limit imposed by K_3. This is also exemplified by the rapid saturation the IPF curve in Fig. 8. The same result applies in the case of Talbot based system as was pointed out recently by Engelhardt *et. al* [21].

Acknowledgements

This work was supported by the Wellcome Trust (085856/Z/08/Z). A. Olivo is supported by a Career Acceleration Fellowship awarded by the UK Engineering and Physical Sciences Research Council (EP/G004250/1).

#127840 - $15.00 USD Received 30 Apr 2010; revised 27 Jul 2010; accepted 29 Jul 2010; published 1 Sep 2010